Available online at www.sciencedirect.com
SCIENCE DIRECT®
Wear 258 (2005) 992–1000
WEAR
www.elsevier.com/locate/wear

Creep forces in simulations of traction vehicles running on adhesion limit

O. Polach*

Bombardier Transportation, CH-8401 Winterthur, Switzerland

Received 13 June 2003; received in revised form 28 November 2003; accepted 1 March 2004

Abstract

A necessary condition for complex simulations of vehicle system dynamics including drive dynamics and traction control when running on adhesion limit, is an advanced creep force modelling taking large longitudinal creep into account. A method presented in the article allows to simulate various real wheel–rail contact conditions using one parameter set. The parameters can be identified from measurements or the recommended parameters for modelling of typical wheel–rail contact conditions in engineering applications can be used. Influence of vehicle speed, longitudinal, lateral and spin creep and shape of the contact ellipse is also considered. The method was validated by comparisons with measurements as presented in application examples.

Keywords: Wheel–rail contact; Wet or contaminated rail; Creep forces; Railway vehicle dynamics; Multi-body simulation; Traction vehicles

1. Introduction

High adhesion utilisation and sophisticated vehicle dynamics design of modern locomotives and traction vehicles demands complex simulations which simultaneously take into consideration the mechanical, electrotechnical and control system fields.

In computer simulations, different methods are used to calculate tangential creep forces between wheel and rail:

- for general vehicle dynamic calculations, without or with small tractive forces;
- for analysis of traction chain dynamics and traction control with high tractive forces.

In vehicle dynamics, small creep values (microslip) are of main importance. Longitudinal and lateral creep as well as spin should be taken into account. The friction coefficient is assumed to be constant. The difference between dry and wet conditions is usually expressed only with the value of the friction coefficient.

In traction chain dynamics usually only the longitudinal direction is taken into account. There is a maximum of creep force–creep function, the so-called adhesion optimum, and a decreasing section behind this maximum. Typical shapes of measured creep force–creep functions for large creep are shown in Fig. 1. The form and the initial slope for wet, dry or polluted conditions are different.

For a complex simulation of dynamic behaviour of locomotive or traction vehicle in connection with drive dynamics and traction control, the different creep force models described above have to be made into one model. A suitable method is described in this article and its application illustrated in examples.

2. A creep force model for simulations of traction vehicles running on adhesion limit

2.1. Overview

A possible explanation of the decreasing section of creep force–creep function for large longitudinal creep is the

* Tel.: +41 52 2641656; fax: +41 52 2641101.
E-mail address: oldrich.polach@ch.transport.bombardier.com.

0043-1648/$ – see front matter © 2004 Elsevier B.V. All rights reserved.
doi:10.1016/j.wear.2004.03.046

Nomenclature

a,b	half-axes of the contact ellipse
A	ratio of friction coefficients μ_∞/μ_0
B	coefficient of exponential friction decrease (s/m)
c_{11}	coefficient from Kalker's linear theory
C	proportionality coefficient characterising the contact shear stiffness (N/m^3)
f_x,f_y	adhesion coefficients in longitudinal (x) and lateral (y) directions $f_x = F_x/Q, f_y = F_y/Q$
F_x,F_y	tangential contact force in longitudinal (x) and lateral (y) directions
G	shear module
k	reduction factor of the coefficients of Kalker's linear theory
k_A	reduction factor in the area of adhesion
k_S	reduction factor in the area of slip
Q	wheel load
s	total creep
s_x,s_y	creep in longitudinal (x) and lateral (y) directions
V	vehicle speed
w	total creep (slip) velocity
$w_x,\ w_y$	creep (slip) velocity in longitudinal (x) and lateral (y) directions

Greek letters

ε	gradient of the tangential stress in the area of adhesion
ε_x	gradient of the tangential stress in longitudinal (x) direction
μ	coefficient of friction
μ_0	maximum friction coefficient at zero slip velocity
μ_∞	friction coefficient at infinity slip velocity
σ	normal stress
τ	tangential stress
τ_{max}	maximum tangential stress
υ_x	non-dimensional longitudinal creep, see [9,28] for definition

decrease of friction coefficient with increasing slip velocity due to increasing temperature in the contact area [1–5]. Another explanation – different friction coefficients in the area of adhesion and area of slip (static and kinematic friction coefficient) – does not seem to sufficiently influence the shape of the creep force curve [6,7].

The assumption of friction coefficient decreasing with increasing temperature usually leads to good agreement between theory and measurements for dry and clean contact conditions. The agreement is worse for contaminated surfaces. For wet conditions, an interfacial layer of liquid should be considered. In spite of several published theories considering a layer of liquid or moisture, there is no simple model existing to simulate dry as well as wet conditions in contact of wheel and rail in computer simulations.

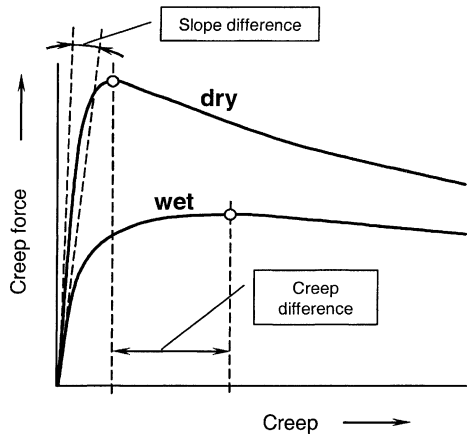

Fig. 1. Typical shape of measured creep force–creep functions and the relation between the initial slope and the maximum for dry and wet contact conditions.

The method described in this article allows to simulate creep forces according to measurements for various contact conditions — dry, wet, polluted, etc. It is based on a fast method for calculation of wheel–rail forces developed by the author and largely tested and used in various three-dimensional multi-body simulation tools. The original method is presented briefly in the next chapter. Then, a possible modelling of friction coefficient decreasing with increasing creep velocity together with the reduction of initial slope of creep force curve will be shown and the limitations of this model explained. Later, an extension by different reduction factors in the area of adhesion and area of slip will be presented and the contact model parameters identified by comparisons with measurements. The extended method allows to model the creep forces in multi-body simulations for various contact conditions in good agreement with the measurements.

2.2. A fast method for calculation of creep forces in multi-body simulation

The method developed by the author for calculation of creep forces in multi-body simulations [8,9] is based on a theoretical model for longitudinal and lateral creep assuming a coefficient characterising the contact shear stiffness. The basic idea is to integrate the shear stress distribution over the contact surface to obtain the magnitude of the resultant creep force F. The different creep force components F_x, F_y are assumed to be proportional to the longitudinal and lateral creepages.

The contact area is assumed elliptical with half-axes a, b and normal stress distribution according to Hertz. The distribution of the tangential stress τ can be seen on Fig. 2. The

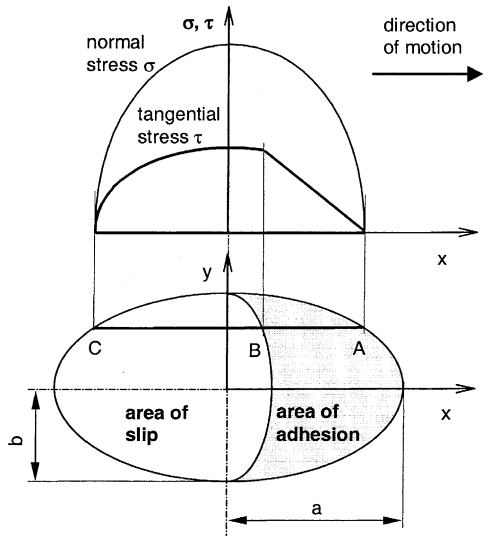

Fig. 2. Distribution of normal and tangential stresses in the wheel–rail contact area in the proposed method.

maximum value of tangential stress at any arbitrary point is

$$\tau_{\max} = \mu\sigma \tag{1}$$

The solution described in [9] leads to the resultant tangential creep force[1] (without spin) as

$$F = \frac{2Q\mu}{\pi}\left(\frac{\varepsilon}{1+\varepsilon^2} + \arctan\varepsilon\right) \tag{2}$$

with

$$\varepsilon = \frac{2}{3}\frac{C\pi a^2 b}{Q\mu}s \tag{3}$$

where C is proportionality coefficient characterising the contact shear stiffness (N/m^3).

The contact shear stiffness coefficient C can be derived from Kalker's linear theory [10]. For the longitudinal direction, we get

$$\varepsilon_x = \frac{1}{4}\frac{G\pi abc_{11}}{Q\mu}s_x \tag{4}$$

where s_x is the longitudinal component of the total creep s

$$s = \sqrt{s_x^2 + s_y^2} \tag{5}$$

$$s_i = \frac{w_i}{V}, \quad i = x, y \tag{6}$$

The forces F_x, F_y in longitudinal and lateral directions are

$$F_i = F\frac{s_i}{s}, \quad i = x, y \tag{7}$$

[1] The force acts against the creep, therefore the right site of the equation should start with a negative sign. For simplification this negative sign is left out in this article.

and the adhesion coefficients

$$f_i = \frac{F_i}{Q}, \quad i = x, y \tag{8}$$

The effect of spin to the lateral creep force is approximated based on integration of the tangential stress caused by pure spin and on the results of Kalker's linear theory. The solution can be used for general conditions of longitudinal, lateral and spin creep. A detailed description and computer code can be found in [9].

Comparisons with other methods used in computer simulations give very good results. Using the contact shear stiffness coefficient C derived from Kalker's linear theory, the method is used as a simple and fast alternative instead of the FASTSIM computer code [11] or other methods or precalculated tables. The method is faster than FASTSIM and approximately as fast as the method developed by Shen et al. [12], but the results are closer to FASTSIM than other methods. The method was implemented into the simulation tools ADAMS/Rail, SIMPACK, GENSYS and used in other tools as user routine as well.

2.3. Friction coefficient dependent on slip velocity

A creep force law with a marked adhesion optimum can be modelled using the friction coefficient decreasing with increasing slip (creep) velocity between wheel and rail [13–15]. The dependence of friction on the slip velocity was observed by various authors and is described, e.g. in [16]. The variable friction coefficient can be expressed by the following equation

$$\mu = \mu_0\left[(1-A)\,\mathrm{e}^{-Bw} + A\right] \tag{9}$$

Where A is the ratio of limit friction coefficient μ_∞ at infinity slip velocity to maximum friction coefficient μ_0

$$A = \frac{\mu_\infty}{\mu_0} \tag{10}$$

In recent years, theoretical studies have been published explaining the decreasing section of creep force–creep function under the influence of temperature in the contact area [1–5]. With increasing creep, the temperature in the contact area increases and the coefficient of friction decreases.

In addition, the reduction $k < 1$ of the initial slope of creep force curve explained in [5,17] through the influence of the surface roughness and in [18,19] by effect of contamination can be used. Using these assumptions, a good agreement between theory and measurements can be found in some cases for dry or slightly contaminated conditions. For wet or polluted conditions however, an interfacial layer of liquid or contaminants should be considered which have not been included in the above theory. A large longitudinal slip between wheel and rail occurs for the adhesion limit, in particular for the maximum transmissible tractive forces.

Using the theory of friction coefficient decreasing with increasing slip by the influence of temperature for the case of

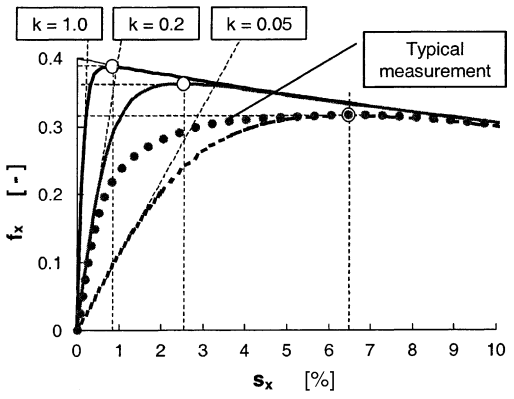

Fig. 3. Calculated creep force–creep functions with decreasing friction coefficient and various reduction factors k of Kalker's coefficients compared with typical measurement on wet or contaminated rail.

wet or polluted contact conditions, the only way to achieve the adhesion optimum at large creep values is a significant reduction of the coefficients of Kalker's linear theory ($k < 0.1$), see Fig. 3. But the measurements of the initial slope of creep force–creep function do not show such low values. Typical values of the reduction factor for real wheel–rail contact conditions as evaluated from measurements in [20–22] are 0.2–0.5 for wet rails and 0.6–0.85 for dry rails. As can be seen on Fig. 3, the only use of decreasing friction coefficient does not allow to simulate the creep forces between wheel and rail in complex dynamics simulations when transmitting the limiting tractive forces under unfavourable adhesion conditions.

An extension of the fast method for calculation of creep forces presented in the next chapter allows to adapt the creep force model for various conditions of wheel–rail contact according to measurements.

2.4. An extended creep force model for large creep applications

The proposed modelling of the real creep forces for wet, contaminated or dry rail can be explained as a combination of dry and wet friction. For small creep values, the area of adhesion extends to the greater part of the contact area. The conditions are similar to dry friction. For large creep values, there is slip in the main part of the contact area. The effect of the interfacial layer of water, pollution or contaminants increases. Consequently, the stiffness of the anisotropic surface layer [18] decreases and, as a result of this, the creep force–creep function reduces its gradient significantly.

To model these conditions, different reduction factors k_A in the area of adhesion and k_S in the area of slip are used. This is easily possible using the proposed method because there are two terms in Eq. (2); the first one related to the area of adhesion and the second to the area of slip. Eq. (2) has then the form

$$F = \frac{2Q\mu}{\pi}\left(\frac{k_A\varepsilon}{1+(k_A\varepsilon)^2} + \arctan(k_S\varepsilon)\right), \quad k_S \le k_A \le 1 \tag{11}$$

Using different reduction factors in the area of adhesion and in the area of slip for a constant friction coefficient there is hardly any reduction of the function gradient at small creepages but a significant reduction of the gradient for large creep near saturation, see Fig. 4.

The gradient of the creep force–creep function at the origin of the coordinates corresponds to the reduction of Kalker's coefficient

$$k = \frac{k_A + k_S}{2} \tag{12}$$

The proposed extension by two reduction factors together with the friction coefficient decreasing with increasing slip (creep) velocity allows to reach the forms of creep force curves for various contact conditions more similar to the measurements than using other methods.

2.5. Parameter identification from measurements

The parameters of the reduction factors k_A, k_S and of the friction coefficient function have to be found by comparison of measured and computed creep force–creep functions for longitudinal direction. It is assumed that the parameters identified for longitudinal direction are valid for lateral direction too. The assumption can be accepted as suitable because

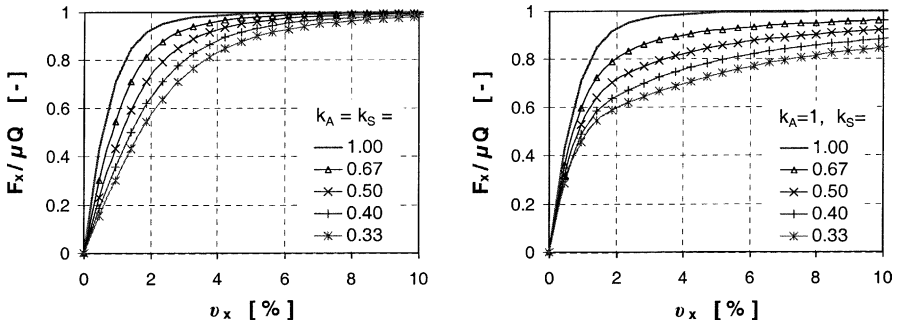

Fig. 4. Reduction of Kalker's coefficients with one factor (left) and using two different reduction factors (right) in the area of adhesion and area of slip in the proposed method (friction coefficient constant).

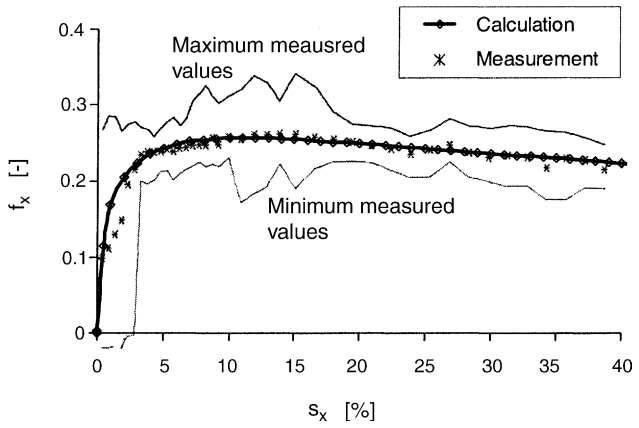

Fig. 5. Model of creep forces based on the measurements with the Bombardier locomotive SBB 460 [22] (wet, $V = 40$ km/h).

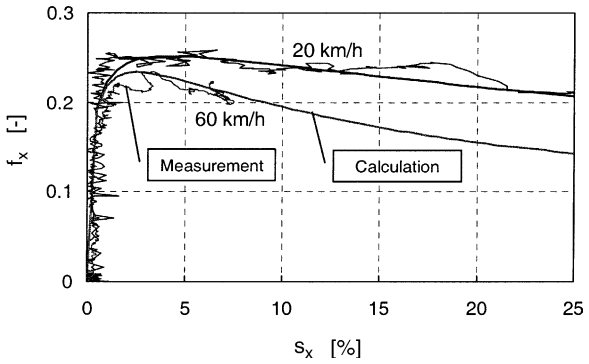

Fig. 6. Model of creep forces based on the measurements with the Bombardier locomotive 12X [23] (wet, $V = 20$ and 60 km/h).

- the parameters identified from measurements influence mainly the forces at large creep;
- large creep occurs mainly in longitudinal direction because of traction or braking; the maximum lateral creep cannot reach the level of maximum longitudinal creep due to traction or braking.

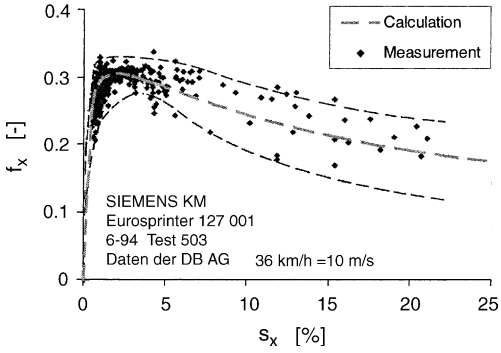

Fig. 8. Model of creep forces based on the measurements with the Siemens locomotive Eurosprinter 127001 [25] (dry, $V = 36$ km/h).

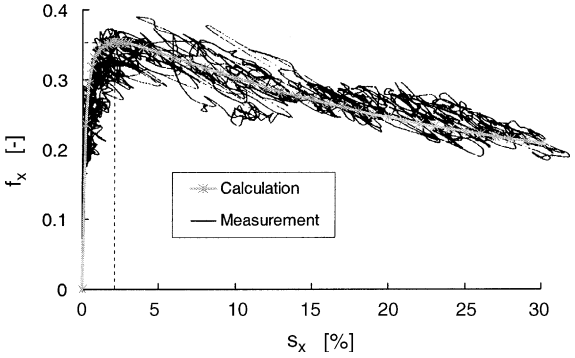

Fig. 9. Model of creep forces based on the measurements with the Siemens locomotive S 252 [26] (dry, $V = 30$ km/h).

Using the proposed method, the following measurements were modelled:

- Measurements with the Bombardier locomotive SBB 460 [22] on artificially watered rails, see Fig. 5. The results of seven measurements with a speed of 40 km/h were classified and average, maximal and minimal values obtained.

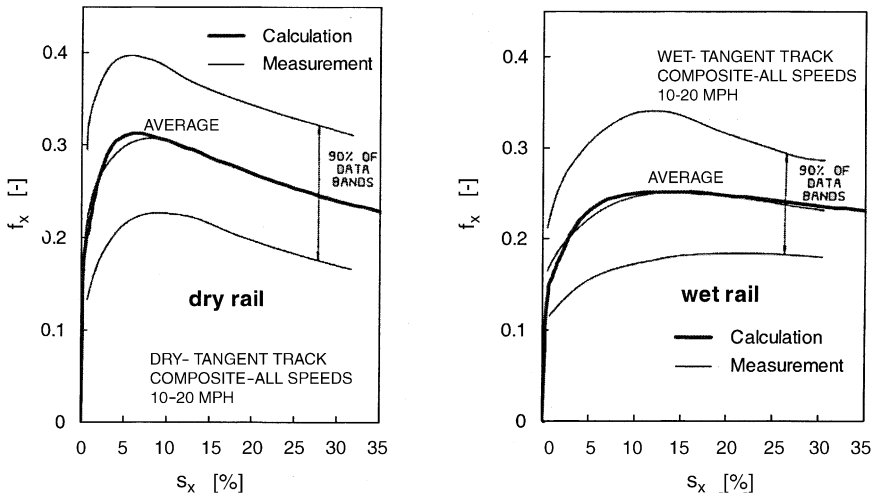

Fig. 7. Model of creep forces based on the measurements with the GM locomotives SD 45X [24] ($V = 16$–32 km/h).

Table 1
Parameters of the extended creep force model identified from measurements

Vehicle	SBB 460	12X	SD45X	SD45X	DB127	S252
Wheel–rail conditions	Wet	Wet	Wet	Dry	Dry	Dry
Speed (km/h)	40	20 and 60	16–32	16–32	36	30
Reference (measurement)	[22]	[23]	[24]	[24]	[25]	[26]
Comparison model-measurement	Fig. 5	Fig. 6	Fig. 7	Fig. 7	Fig. 8	Fig. 9
Model parameter						
k_A	0.16	0.65	0.29	0.68	0.72	1.00
k_S	0.07	0.26	0.07	0.14	0.36	0.50
μ_0	0.31	0.28	0.30	0.40	0.36	0.40
A	0.50	0.40	0.38	0.44	0.38	0.36
B (s/m)	0.16	0.40	0.18	0.60	0.70	0.55

Table 2
Typical model parameters for dry and wet conditions of real wheel–rail contact

Model parameter	Wheel–rail conditions	
	Dry	Wet
k_A	1.00	0.30
k_S	0.40	0.10
μ_0	0.55	0.30
A	0.40	0.40
B (s/m)	0.60	0.20

- Measurements with the Bombardier test locomotive 12X [23] on artificially watered rails with speeds of 20 and 60 km/h (Fig. 6).
- Measurements on GM locomotives SD 45X in the USA [24], wet and dry contact conditions, average values and 90% data bands of measurements with speeds between 16 and 32 km/h (Fig. 7).
- Measurements with the Siemens locomotive DB 127 Eurosprinter (according to [25]), dry rails, speed 36 km/h (Fig. 8).
- Measurements with the Siemens locomotive S 252 (according to [26]), dry rails, speed 30 km/h (Fig. 9).

The parameters of creep force models are shown in Table 1. Comparing the above presented models based on various measurements we can observe some similarities in model parameters. Typical values of model parameters for dry and wet conditions are presented in Table 2 and Fig. 10. The model with parameters according to Table 2 is in good agreement with creep force–creep functions used as typical for investigation of traction control in [27].

The presented model can be used for any speed, from very small values when starting up to high speed values, using one parameter set for certain wheel–rail conditions. It was verified by comparisons with measurements for speeds up to 100 km/h. The model is not limited to one speed or to a certain creep range. In this way, the influence of speed on the form and maximum of creep force–creep functions is expressed with only one parameter set, see Fig. 11. Besides this, the influence of longitudinal, lateral and spin creep as well as the shape of the contact ellipse is also taken into account (Fig. 12). Of course, a change of surface conditions (dry, wet, etc.) as well as other effects, e.g. the cleaning effect due to large longitudinal creep (so-called rail conditioning), will need a change of model parameters.

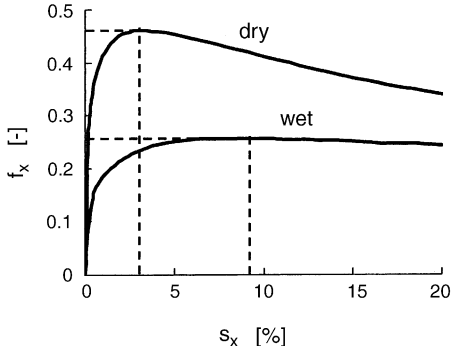

Fig. 10. Calculated creep force–creep functions for typical parameters of real wheel–rail contact (Table 2) for dry and wet conditions.

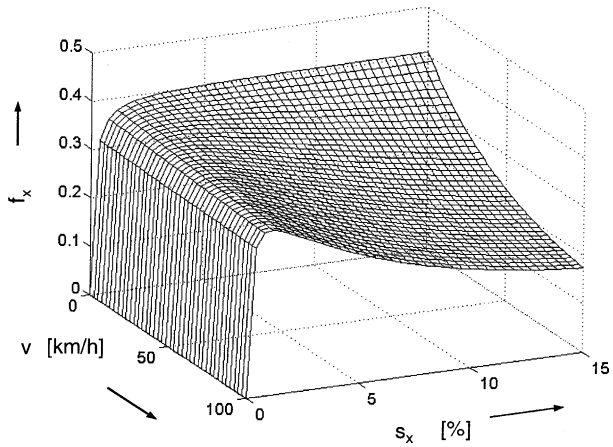

Fig. 11. Influence of vehicle speed on the form of creep force–creep functions for longitudinal direction; model parameters according to measurements in Fig. 9.

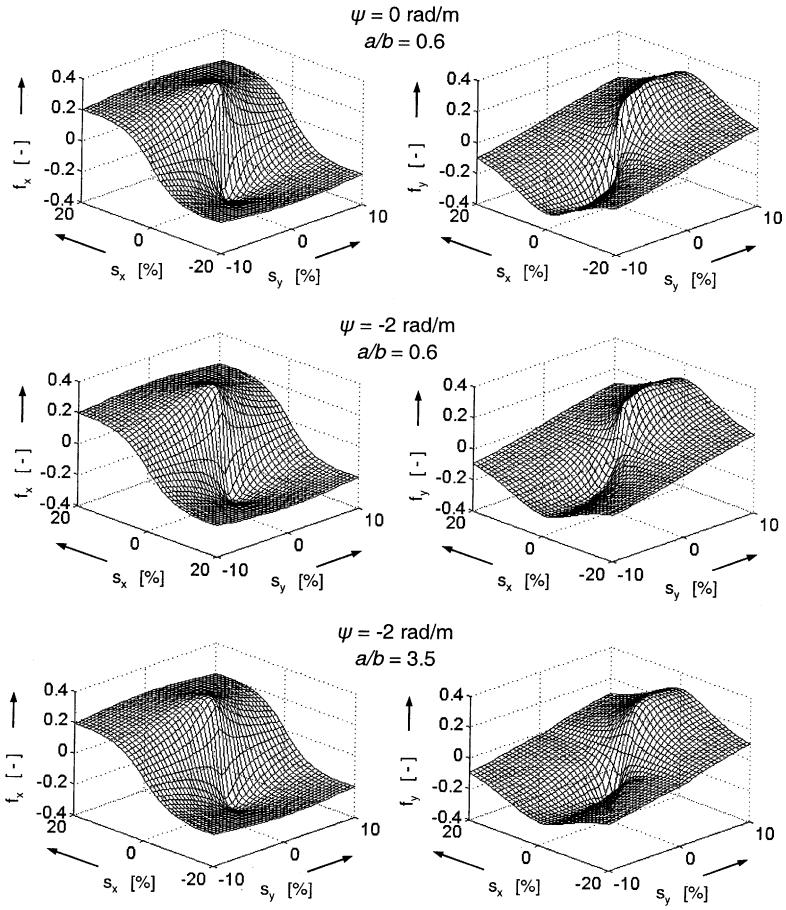

Fig. 12. Creep forces according to the proposed extended method in function of longitudinal (s_x), lateral (s_y) and spin (ψ) creepages as well as of the form of the contact area (a/b); model parameters according to measurements in Fig. 9, $V = 30$ km/h.

3. Model validation by comparison of simulations and measurements

3.1. Influence of tractive force on the steering of a self-steering bogie

In order to test the possibility of simulating the dynamic change of traction torque, a test case used during the adhesion test [22] of the four axle SBB 460 locomotive of the Swiss Federal Railways was simulated. The locomotive design combines very good curving performance with high maximum speed due to the coupling of wheelsets, realised by a mechanism with a torsional shaft assembled to the bogie frame. The locomotive model in simulation tool ADAMS/Rail consists of 51 rigid bodies and contains 266 d.f.

In the course of curving simulation, the traction torque was increased from zero to the adhesion limit, in a similar way as during the adhesion test measurements. In this manner, a run on the unstable (decreasing) section of creep force curve was simulated [28]. With increasing tractive effort, the wheelset steering ability decreases. Simultaneously, the first wheelset of the bogie moves to the inner rail. The calculated steering angle between the wheelsets as a function of tractive force in the steering linkages is compared with measurement in Fig. 13. The comparison confirms a good agreement in the tendency although the real track irregularity is not known in detail.

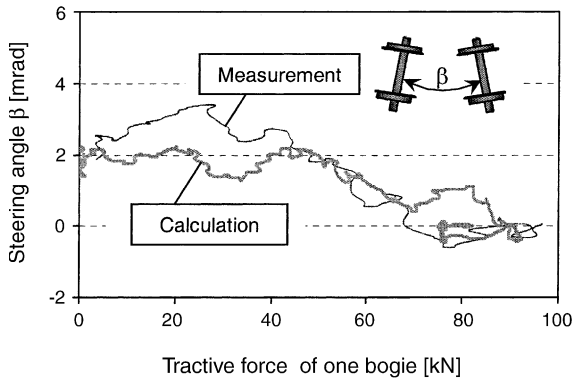

Fig. 13. Comparison of the measured and calculated steering angle between wheelsets as function of tractive effort of a single bogie.

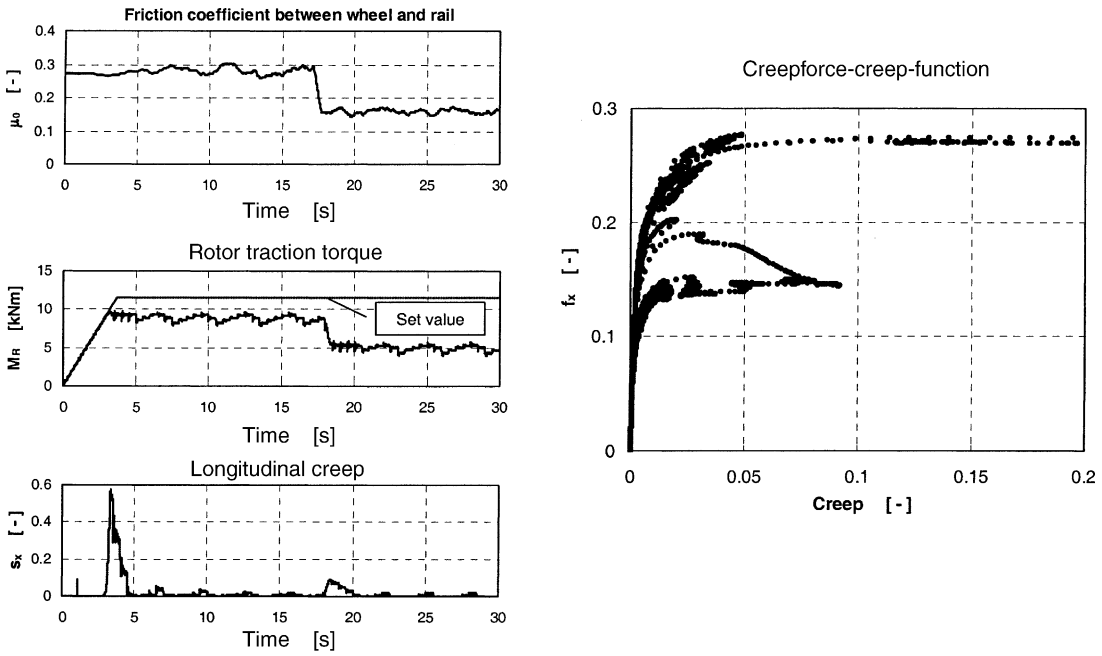

Fig. 14. Rotor torque, longitudinal creep between wheel and rail and creep force–creep-diagram as a co-simulation results of sudden worsening of adhesion conditions modelled by reduction of friction coefficient.

3.2. Co-simulation of vehicle dynamics and traction control

In following two application examples, the creep force model described above was used in a co-simulation of vehicle dynamics and traction control under bad adhesion conditions. The vehicle model is represented by the locomotive 12X of Bombardier Transportation modelled in the simulation tool SIMPACK. The controller was modelled in computer code MATLAB-SIMULINK. During co-simulation, both programmes are running in parallel exchanging few channels only, see [23,29] for details.

Fig. 14 shows a simulation of traction control reaction following a sudden worsening of adhesion conditions, see the input function of friction coefficient between wheel and rail in Fig. 14. Besides the sudden reduction of friction coefficient after approx. 30 m of track, small stochastic oscillations are superimposed. The torque on the rotor cannot reach the

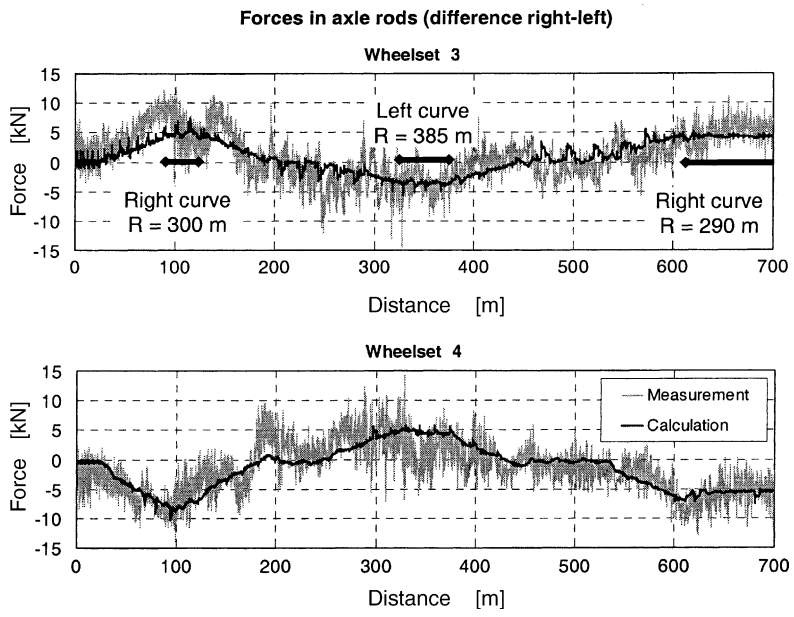

Fig. 15. Comparison of measured (non-filtered) and calculated forces in the longitudinal axle guidance during a start and acceleration of a test locomotive on a curved track.

set value because of bad wheel–rail adhesion. The maximum achievable value is obtained by means of an adaptive traction controller. After the sudden reduction of friction coefficient, the creep first increases, but the controller stabilises the working point at a new adhesion optimum with low creepage after a short transition period.

Another co-simulation study shows a starting and acceleration of locomotive hauling a train on a curved sloping track. Fig. 15 presents a comparison of measurement and simulation of longitudinal forces in wheelset linkages. The observed forces on the straight track and on the left and right curves are very close in measurement and simulation. The comparison validates the proposed method as suitable for computer simulation of traction vehicles running on adhesion limit.

4. Conclusion

The proposed method for calculation of wheel–rail forces enables computer simulations of complex vehicle system dynamics including running and traction dynamics for large traction creep when running on adhesion limit. It allows to simulate various wheel–rail contact conditions using one parameter set for various speeds. Influence of longitudinal, lateral and spin creep and shape of the contact ellipse is also considered.

Measurements with five locomotives under different weather and wheel–rail conditions were modelled and the model input parameters are presented. The method can be used to model the creep forces based on the measured creep force–creep functions. If no measurements are available, the parameters recommended for typical wheel–rail contact conditions can be used in engineering applications. The method was used in complex simulations of adhesion tests and traction control during an acceleration on curved lines and validated by comparisons with measurements.

References

[1] J. Holland, F. Rick, Einfluss der Kontakttemperatur auf den Kraftschlussbeiwert, Tribologie und Schmierungstechnik 44 (1997) 73–78.
[2] F. Rick, Zur Erfassung der Geschwindigkeitsabhängigkeit des Kraftschlussbeiwertes eines hochbelasteten Rad-Schiene-Kontaktes, Thesis, Technical University Clausthal, Germany, 1998.
[3] H. Schwarze, Geschwindigkeitsabhängiger Kraftschluss hochbelasteter Rad-Schiene-Kontakte, Elektrische Bahnen 99 (2001) 203–218.
[4] K. Hou, J. Kalousek, Thermal effect on adhesion in wheel/rail interface, in: Proceedings of the Fifth International Conference Contact Mechanics and Wear of Rail Wheel Systems, Tokyo, Japan, July 25–28, 2000, pp. 239–244.
[5] M. Ertz, F. Bucher, Improved creep force model for wheel/rail contact considering roughness and temperature, Vehicle Syst. Dyn. Suppl. 37 (2002) 314–325.
[6] T. Ohyama, Some basic studies on the influence of surface contamination on adhesion force between wheel and rail at higher speeds, Q. Rep. Railway Tech. Res. Inst. 30 (1989) 127–135.
[7] J.B. Nielsen, A. Theiler, Tangential contact problem with friction coefficients depending on sliding velocity, in: Proceedings of the Second Mini Conference on Contact Mechanics and Wear of Rail/Wheel Systems, Budapest, July 29–31, 1996, pp. 44–51.
[8] O. Polach, Solution of wheel–rail contact forces suitable for calculation of rail vehicle dynamics, in: Proceedings of the Second Int. Conference on Railway Bogies, Budapest, September 14–16, 1992, pp. 10–17.
[9] O. Polach, A fast wheel–rail forces calculation computer code, Vehicle Syst. Dyn. Suppl. 33 (1999) 728–739.
[10] J.J. Kalker, On the rolling contact of two elastic bodies in the presence of dry friction, Thesis, Delft, 1967.
[11] J.J. Kalker, A fast algorithm for the simplified theory of rolling contact, Vehicle Syst. Dyn. 11 (1982) 1–13.
[12] Z.Y. Shen, J.K. Hedrick, J.A. Elkins, A comparison of alternative creep force models for rail vehicle dynamic analysis, in: Proceedings of the 8th IAVSD Symposium, Cambridge, MA, August 15–19, 1983, pp. 591–605.
[13] P. Häse, S. Menth, Kraftschluss bei Triebfahrzeugen – Modellbildung und Verifikation an Messdaten, Elektrische Bahnen 94 (1996) 125–134.
[14] O. Polach, Rad-Schiene-Modelle in der Simulation der Fahrzeug- und Antriebsdynamik, Elektrische Bahnen 99 (2001) 219–230.
[15] W. Zhang, J. Chen, X. Wu, X. Jin, Wheel/rail adhesion and analysis by using full scale roller rig, Wear 253 (2002) 82–88.
[16] I.V. Kragelski, M.N. Dobyčin, V.S. Kombalov, Friction and Wear: Calculation Methods, Pergamon Press, Oxford, 1982.
[17] F. Bucher, K. Knothe, A. Theiler, Normal and tangential contact problem of surfaces with measured roughness, Wear 253 (2002) 204–218.
[18] J.J. Kalker, Über die Mechanik des Kontaktes zwischen Rad und Schiene, ZEV-Glasers Annalen. 102 (1978) 214–218.
[19] H. Harrison, T. Mccanney, J. Cotter, Recent developments in COF measurements at the rail/wheel interface, in: Proceedings of the 5th International Conference Contact Mechanics and Wear of Rail Wheel Systems, Tokyo, Japan, July 25–28, 2000, pp. 30–35.
[20] H. Fiehn, M. Weinhardt, N. Zeevenhooven, Drehstromversuchsfahrzeug der Niederländischen Eisenbahnen – Adhäsionsmessungen, Elektrische Bahnen 77 (1979) 329–338.
[21] H.H. Vogel, SBB 450 Adhäsionsverhalten, Techn. Report No. 401, SLM Winterthur, 1991.
[22] O. Polach, SBB 460 Adhäsionsversuche, Techn. Report No. 414, SLM Winterthur, 1992.
[23] O. Polach, Optimierung moderner Lok-Drehgestelle durch fahrzeugdynamische Systemanalyse, Eisenbahningenieur 53 (2002) 50–57.
[24] C.F. Logston Jr., G.S. Itami, Locomotive friction-creep studies, ASME J. Eng. Ind. 102 (1980) 275–281.
[25] B. Engel, H.P. Beck, J. Alders, Verschleißreduzierende Radschlupfregelung mit hoher Kraftschlussausnutzung, Elektrische Bahnen 96 (1998) 201–209.
[26] W. Lang, G. Roth, Optimale Kraftschlussausnutzung bei Hochleistungs-Schienenfahrzeugen, Eisenbahntechnische Rundschau 42 (1993) 61–66.
[27] R. Schreiber, R. Kögel, P. Häse, P. Hildenbrand, Regelung zur optimalen Kraftschlussausnutzung bei Drehstromlokomotiven auf der Basis der Steigung der Kraftschlusskennlinien, Elektrische Bahnen 93 (1995) 157–163.
[28] O. Polach, Influence of locomotive tractive effort on the forces between wheel and rail, Selected papers from the 20th International Congress of Theoretical and Applied Mechanics held in Chicago, 28 August–1 September, 2000, Vehicle Syst. Dyn. Suppl. 35 (2001) 7–22.
[29] C. Kossmann, Design calculation and verification using SIMPACK Wheel/Rail at Bombardier Transportation Winterthur, SIMPACK User Meeting, 13–14. 11. 2001. Bad Ischl, Austria, in Internet: http://www.simpack.de/.